2021 IEEE International Conference on Robotics and Automation (ICRA 2021)
May 31 - June 4, 2021, Xi'an, China

Generalized Point Set Registration with the Kent Distribution

Zhe Min, *Member*, *IEEE*, Delong Zhu, *Member*, *IEEE*, Max Q.-H. Meng*, *Fellow of IEEE*,

***Abstract*— Point set registration (PSR) is an essential problem in communities of computer vision, medical robotics and biomedical engineering. This paper is motivated by considering the anisotropic characteristics of the error values in estimating both the positional and orientational vectors from the PSs to be registered. To do this, the multi-variate Gaussian and Kent distributions are utilized to model the positional and orientational uncertainties, respectively. Our contributions of this paper are three-folds: (i) the PSR problem using normal vectors is formulated as a maximum likelihood estimation (MLE) problem, where the anisotropic characteristics in both positional and normal vectors are considered; (ii) the matrix forms of the objective function and its associated gradients with respect to the desired parameters are provided, which can facilitate the computational process; (iii) two approaches of computing the normalizing constant in the Kent distribution are compared. We verify our proposed registration method on various PSs (representing pelvis and femur bones) in computer-assisted orthopedic surgery (CAOS). Extensive experimental results demonstrate that our method outperforms the state-of-the-art methods in terms of the registration accuracy and the robustness.**

I. Introduction

Registration is a common and fundamental problem in computer vision, computer graphics, robotics and biomedical engineering communities [1]–[7]. The objective of registration is to accurately estimate the spatial transformation (either rigid or non-rigid) and to recover the point correspondences between two spaces [8]–[14]. The two spaces can be represented with volumetric images or distinctive features (e.g. points, lines or planes) [15], [16]. In medical image analysis, registration technique is adopted to align multiple images representing the same organs (either from the same or different patients) into one common coordinate frame[17], [18]. For example, the pre-operative rigid registration of different imaging modalities, such as Magnetic Resonance Imaging (MRI) and computed tomography (CT), provides the robust fusion of soft tissue information with accurate bone delineation for neurosurgical planning [19]–[21]. As indicated in [22], over the past 30 years, we have seen the significant emergence of systems that incorporate medical imaging, robots, and other technologies to enhance patient care's quality. Computer-assisted interventions (CAIs) or computer-assisted surgery (CAS) provides surgeons with additional digital information of the patient [2], [23], [24]. Before surgery, the patient usually goes for a CT or MRI scanning to acquire a patient specific 3D model [25]. During surgery, the information together with the pre-operative patient model has to be combined with the intra-operative images, video cameras or robots [26]–[28].

This paper is organized as follows: Section II reviews the related registration algorithms; Section III describes the motivation and contributions of this paper; Section IV formulates the registration problem; Section V presents the details of the expectation maximization (EM) procedures; Section VI introduces the implementation details; Section VII describes the experimental results; Section VIII concludes the paper.

Zhe Min is with the University College London, London, UK. Zhe Min and Delong Zhu were with the Department of Electronic Engineering, The Chinese University of Hong Kong, N.T., Hong Kong SAR, China.

Max Q.-H. Meng is with the Department of Electronic and Electrical Engineering, Southern University of Science and Technology, Shenzhen, China, and also with the Shenzhen Research Institute, The Chinese University of Hong Kong, Shenzhen, China, on leave from the Department of Electronic Engineering, Hong Kong (e-mail: max.meng@ieee.org)

This project is partially supported by the Hong Kong RGC GRF grants #14210117, Hong Kong RGC NSFC/RGC Joint Research Scheme #N_CUHK448/17, and Shenzhen Science and Technology Innovation projects JCYJ20170413161616163 awarded to Max Q.-H. Meng.

*Corresponding Author

II. Related Work

Among the existing various registration methods, iterative closest point (ICP) is perhaps the most well known one. ICP is an iterative algorithm that first finds the best correspondence and then updates the transformation with current updated correspondences [29]. Euclidean distance is used as the objective function in both correspondence and registration steps. Notably, in the original ICP, one-to-one hard correspondence strategy is adopted. The performance of ICP is susceptible to the initial transformation and outliers, and easily converges to a local minima while it proves to be accurate and fast in many cases. Built upon the ICP method and the branch-and-bound (BnB) technique that can search the 3D motion space SE(3) efficiently, Yang et al. have proposed the Go-ICP method that can find the globally optimal solution [30]. To make ICP robust to noise and outliers, different variants of ICP have been developed [31].

On the other hand, the main idea of probabilistic methods is to represent one PS with a density function and minimize some 'distance' of the densities. The other key idea of GMM-based registration methods is that the multiply-link correspondence strategy is usually used between two PSs. More specifically, each point in the *data* PS can be interpreted as being generated by some Gaussian with a specific isotropic covariance. Each point in the *mode* PS, on the other hand, is considered as the mixtures' mean. Under the probabilistic framework, the iterations of finding correspondences and updating transformations in the ICP method are reconsidered as a type of EM procedure. In E-step, the expectation over *latent* correspondence variables is calculated. In M-step, under the current correspondences, maximization of *complete log-liklihood* is conducted over the registration parameters. The two steps iterate until the algorithm converges *or* a maximum number of iterations is reached.

In the Coherent Point Drift (CPD) algorithm [32], the registration of PSs is formulated as a probability density estimation problem. With the assumption of isotropic covariance in the data PS, the optimal rotation matrix can be solved in a closed-form solution in M-step with the singular value decompostion (SVD) technique. Expectation Conditional Maximization Point Registration (ECMPR) [33] extends the CPD's isotropic covariance to anisotropic covariance matrix. In the ECM steps, each M-step in the CPD method is replaced by a sequence of conditional maximization steps or *CM-steps*. More specifically, during each *CM-step*, one registration parameter is optimized conditioned by that the other parameters are constants. Estimating the current rigid transformation matrix in *CM-steps* is reformulated as a quadratic optimization problem and solved using semidefinite relaxation technique. Motivated by enabling mapping and navigation for the robots in dark, complex, and unstructured environments such as caves and mines, Tabib et al. have proposed the GMM-based registration method that minimizes the L2-norm between two distributions *through* an on-manifold parameterization of the objective function [34]. Their results in the cluttered environments demonstrate superior performance compared to the state of the art methods [34].

Joint Registration of Multiple Point Sets (JRMPC)[35] was proposed to eliminate the bias towards one PS in the pair-wise registration problem. In JRMPC, each PS is assumed to be a realization of a *common* GMM. The joint registration of multiple PSs is formulated as a probabilistic clustering problem. Using the EM scheme, both the GMM parameters and the rigid transformations that relate each individual PS with underlying reference set are estimated. As a by-product, the noise-free underlying reference PS (*model data*) is acquired afterwards. JRMPC algorithm outperforms all the other state-of-the-art registration methods with respect to different percentages of outliers. It should be noted that the covariance matrix is still considered to be isotropic in the JRMPC algorithm. Various registration methods have been proposed to enhance the registration's robustness to noise and outliers [36]–[38]. For example, Yang et al. have proposed a novel registration method that is very robust to a large amount of outliers in a polynomial time [36].

Deep learning methods first learn to encode PSs with high-dimensional features, and then match keypoints to generate correspondence and optimize over the space of rigid transformations [39]–[43]. For example, PointNetLK uses PointNet to learn feature representation and iteratively align the features representations [44]. However, current deep-learning based methods fail to produce acceptable inlier rates [45].

More recently, researchers have proposed the normal-assisted rigid PSR methods under the EM framework [46]–[49]. The isotropic error in determining the normal vectors is assumed in [46], [47], [50]. There are also normal-based registration methods under the ICP framework, and thus may not very robust to outliers [51], [52]. In this paper, the normal-assisted registration problem is solved under the EM framework while *both* the positional error *and* the orientational error are assumed to be anisotropic in 3D space.

III. Motivations and Contributions

Our presented work is motivated by improving the registration's robustness to noise and outliers by (i) incorporating the orientational information (i.e., normal vectors) associated with each point into PSR [51], [53]; (2) considering the anisotropic charactersitics in both positional and normal vectors. Our contributions in this paper can be summarized as follows: (1) The generalized rigid PSR problem is formulated as a maximum likelihood (ML) problem, where the positional and normal error vectors are modelled with multivariate Gaussian and Kent distributions respectively. (2) The gradients of the objective function(also with matrix form) with respect to the desired parameters are computed and provided. (3) We evaluate with extensive experiments the two methods of computing the normalizing constants involved in the Kent distribution, one is the exact form while the other is an approximate one.

IV. Problem Formulation

This paper obeys the following notation conventions. Assume $\mathbf{x}_n,\ \mathbf{y}_m \in \mathbb{R}^3 (n, m \in \mathbb{N}^+)$ are two arbitrary points from the two point sets (PSs) and the unit vectors $\widehat{\mathbf{x}}_n,\ \widehat{\mathbf{y}}_m \in \mathbb{R}^3$ are the associated unit normal vectors (i.e., orientation vectors), where $|\widehat{\mathbf{x}}_n| = 1$ and $|\widehat{\mathbf{y}}_m| = 1$. The points in $\mathbf{Y} = [\mathbf{y}_1, ..., \mathbf{y}_m, ..., \mathbf{y}_M] \in \mathbb{R}^{3\times M}$ are considered as the GMM centroids while the points in $\mathbf{X} = [\mathbf{x}_1, ..., \mathbf{x}_n, ..., \mathbf{x}_N] \in \mathbb{R}^{3\times N}$ are generated by the GMM. In other words, the vectors in $\widehat{\mathbf{Y}} = [\widehat{\mathbf{y}}_1, ..., \widehat{\mathbf{y}}_m, ..., \widehat{\mathbf{y}}_M] \in \mathbb{R}^{3\times M}$ represent the mean directions of the kent mixture model (KMMs) while the vectors in $\widehat{\mathbf{X}} = [\widehat{\mathbf{x}}_1, ..., \widehat{\mathbf{x}}_n, ..., \widehat{\mathbf{x}}_N] \in \mathbb{R}^{3\times M}$ are normal vectors generated from KMMs. Briefly speaking, the generalized (rigid) point set registration (PSR) is to estimate the rigid transformation matrix given the two generalized PSs $\mathbf{D}_x = [\mathbf{X}, \widehat{\mathbf{X}}] \in \mathbb{R}^{6\times N}$ and $\mathbf{D}_y = [\mathbf{Y}, \widehat{\mathbf{Y}}]^{6\times M}$. The probability density function (PDF) of the mixed model is $p(\mathbf{d}_n) = \sum_{m=1}^{M+1} P(m)p(\mathbf{d}_n|z_n = m)$, where $\mathbf{d}_n = [\mathbf{x}_n^\intercal, \widehat{\mathbf{x}}_n^\intercal]^\intercal \in \mathbb{R}^6$ is the six-dimensional directional vector in the data PS is

$$p(\mathbf{d}_n|z_n = m) = \underbrace{\frac{1}{(2\pi)^{\frac{3}{2}}|\mathbf{\Sigma}|^{\frac{1}{2}}} e^{-\frac{1}{2}\left(\mathbf{x}_n-(\mathbf{R}\mathbf{y}_m+\mathbf{t})\right)^\intercal \mathbf{\Sigma}^{-1}\left(\mathbf{x}_n-(\mathbf{R}\mathbf{y}_m+\mathbf{t})\right)}}_{\text{Positional Part}} \underbrace{\frac{1}{c(\kappa,\beta)} e^{\kappa(\mathbf{R}\widehat{\mathbf{y}}_m)^\intercal\widehat{\mathbf{x}}_n+\beta\left(\left((\mathbf{R}\widehat{\boldsymbol{\gamma}}_{1m})^\intercal\widehat{\mathbf{x}}_n\right)^2-((\mathbf{R}\widehat{\boldsymbol{\gamma}}_{2m})^\intercal\widehat{\mathbf{x}}_n)^2\right)}}_{\text{Orientational Part}} \tag{1}$$

where $c(\kappa, \beta) \in \mathbb{R}$ is the normalizing constant of the common Kent distribution [54], $k \in \mathbb{R}$ is the concentration parameter, $\beta \in \mathbb{R}$ determines the ellipticity of the contours of equal probability, $\widehat{\boldsymbol{\gamma}}_{1m} \in \mathbb{R}^3$ and $\widehat{\boldsymbol{\gamma}}_{2m} \in \mathbb{R}^3$ are the major and minor axes associated with m-th model point, and $\mathbf{\Sigma} \in \mathbb{S}^3$ denotes the positional covariance matrix. To account for noise and outliers existing in the data PS $\mathbf{D}_x$, an additional uniform distribution $p(\mathbf{d}_n|z_n = M+1) = \frac{1}{N}$ is added to the original model $p(\mathbf{d}_n)$. Equal membership probabilities $P(m) = \frac{1}{M}$ are assumed for all remaining KMM components ($m = 1, \cdots, M$). Then the mixture model $p(\mathbf{d}_n)$ is:

$$p(\mathbf{d}_n) = w\frac{1}{N} + (1-w)\sum_{m=1}^{M}\frac{1}{M}\underbrace{p(\mathbf{d}_n|z_n = m)}_{p(\mathbf{d}_n|m)} \quad (2)$$

where $0 \leq w \leq 1$ denotes the weight of the uniform distribution, $z_n \in \mathbb{N}^+$ is the correpondence variable. To find the optimal estimation of PDF of mixture models, the accumulative *negative log-likelihood* function is minimized

$$E(\mathbf{R}, \mathbf{t}, \kappa, \beta, \mathbf{\Sigma}, \widehat{\boldsymbol{\gamma}}_{1m}, \widehat{\boldsymbol{\gamma}}_{2m}) = -\sum_{n=1}^{N}\log\sum_{m=1}^{M+1}P(m)p(\mathbf{d}_n|m) \quad (3)$$

V. EM-Based Registration Framework

Expectation Maximization (EM) algorithm is adopted to find the parameters $\mathbf{\Theta} = \{\mathbf{R}, \mathbf{t}, \kappa, \mathbf{\Sigma}, \beta, \widehat{\boldsymbol{\gamma}}_{1m}, \widehat{\boldsymbol{\gamma}}_{2m}\}$ iteratively. As indicated in [32], the idea of EM is to first guess the values of parameters and then use Bayes' theorem to compute a posterior probability distributions $P^{old}(m|\mathbf{d}_n)$ of mixture components that is the expectation or E-step of the algorithm. The new parameter values are then found by minimizing the expectation of the *total negative log-likelihood* function [55]:

$$Q(\mathbf{\Theta}) = -\sum_{n=1}^{N}\sum_{m=1}^{M+1}P^{old}(m|\mathbf{d}_n)\log\Big(P^{new}(m)p^{new}(\mathbf{d}_n|m)\Big) \quad (4)$$

with respect to the "new" parameters, which is the M-step of the algorithm. The Q (i.e. the objective function) is the upper bound of the *negative log-likelihood* function in (3). The GMMs' centroids and KMMs' mean directions are transformed by rotation and translation ($\mathbf{R}$, $\mathbf{t}$). Ignoring constants independent of $\mathbf{\Theta} = \{\mathbf{R}, \mathbf{t}, \kappa, \beta, \mathbf{\Sigma}, \widehat{\boldsymbol{\gamma}}_{1m}, \widehat{\boldsymbol{\gamma}}_{2m}\}$, $Q(\mathbf{\Theta})$ in (4) is rewritten as

$$\begin{aligned}
&Q(\mathbf{R}, \mathbf{t}, \kappa, \beta, \mathbf{\Sigma}, \widehat{\boldsymbol{\gamma}}_{1m}, \widehat{\boldsymbol{\gamma}}_{2m}) = \\
&\sum_{n=1}^{N}\sum_{m=1}^{M}p_{mn}\frac{1}{2}\big(\mathbf{x}_n - (\mathbf{R}\mathbf{y}_m + \mathbf{t})\big)^{\mathsf{T}}\mathbf{\Sigma}^{-1}\big(\mathbf{x}_n - (\mathbf{R}\mathbf{y}_m + \mathbf{t})\big) \\
&-\beta\sum_{n=1}^{N}\sum_{m=1}^{M}p_{mn}(\widehat{\boldsymbol{\gamma}}_{1m}^{\mathsf{T}}\mathbf{R}^{\mathsf{T}}\widehat{\mathbf{x}}_n)^2 + \beta\sum_{n=1}^{N}\sum_{m=1}^{M}p_{mn}(\widehat{\boldsymbol{\gamma}}_{2m}^{\mathsf{T}}\mathbf{R}^{\mathsf{T}}\widehat{\mathbf{x}}_n)^2 \\
&-\kappa\sum_{n=1}^{N}\sum_{m=1}^{M}p_{mn}(\mathbf{R}\widehat{\mathbf{y}}_m)^{\mathsf{T}}\widehat{\mathbf{x}}_n + N_p\log c(\kappa, \beta) + \frac{1}{2}N_P\log|\mathbf{\Sigma}|
\end{aligned} \quad (5)$$

where $p_{mn} = P^{old}(z_n = m|\mathbf{d}_n)$, $N_{\mathbf{p}} = \sum_{n=1}^{N}\sum_{m=1}^{M}p_{mn}$.
Expectation Step The posterior possibility $P^{old}(m|\mathbf{d}_n) = p_{mn}$ is a soft assignment that indicates to what degree $[\mathbf{x}_n^{\mathsf{T}}, \widehat{\mathbf{x}}_n^{\mathsf{T}}]^{\mathsf{T}}$ corresponds to $[\mathbf{y}_m^{\mathsf{T}}, \widehat{\mathbf{y}}_m^{\mathsf{T}}]^{\mathsf{T}}$ and is calculated by applying Bayes' rule:

$$p_{mn}^q = \frac{P(m)p(\mathbf{d}_n|z_n = m)}{p(\mathbf{d}_n)} \quad (6)$$

where the terms $p(\mathbf{d}_n|z_n = m)$ and $p(\mathbf{d}_n)$ are defined in (1) and (2) respectively, $q \in \mathbb{N}$ is the index of iteration. Afterwards, the sum of the posterior probabilities after the q-th step is computed as follows, $N_p^q = \sum_{n=1}^{N}\sum_{m=1}^{M}p_{mn}^q$.
Maximization Step The objective function is further modified by substituting the terms $\mathbf{R}$ in (5) with $d\mathbf{R}\mathbf{R}^{q-1}$, where $d\mathbf{R} \in SO(3)$ denotes the *incremental* rigid transformation between two iterated steps while $\mathbf{R}^{q-1} \in SO(3)$ represents the rigid transformation in the last EM step.

$$\begin{aligned}
&Q(d\mathbf{R}, d\mathbf{t}, \kappa, \beta, \mathbf{\Sigma}, \widehat{\boldsymbol{\gamma}}_{1m}, \widehat{\boldsymbol{\gamma}}_{2m}) = \\
&\sum_{n,m}^{N,M}\underbrace{p_{mn}^q\frac{1}{2}\mathbf{z}_{mn}^{\mathsf{T}}\mathbf{\Sigma}^{-1}\mathbf{z}_{mn}}_{\mathbf{C}_{P,mn}} + N_p^q\log c(\kappa, \beta) + \frac{1}{2}N_P^q\log|\mathbf{\Sigma}| \\
&-\sum_{n,m}^{N,M}\underbrace{\beta p_{mn}^q\big((\widehat{\boldsymbol{\gamma}}_{1m}^{\mathsf{T}}(\mathbf{R}^q)^{\mathsf{T}}\widehat{\mathbf{x}}_n)^2 - (\widehat{\boldsymbol{\gamma}}_{2m}^{\mathsf{T}}(\mathbf{R}^q)^{\mathsf{T}}\widehat{\mathbf{x}}_n)^2}_{\mathbf{C}_{O,mn1}\in\mathbb{R}}\big) \\
&-\sum_{n,m}^{N,M}\underbrace{\kappa p_{mn}^q(d\mathbf{R}\mathbf{R}^{q-1}\widehat{\mathbf{y}}_m)^{\mathsf{T}}\widehat{\mathbf{x}}_n}_{\mathbf{C}_{O,mn2}\in\mathbb{R}}
\end{aligned} \quad (7)$$

where $\mathbf{z}_{mn} = \mathbf{x}_n - d\mathbf{R}(\mathbf{R}^{q-1}\mathbf{y}_m + \mathbf{t}^{q-1}) - d\mathbf{t}$, $\mathbf{R}^q = d\mathbf{R}\mathbf{R}^{q-1}$. The matrix form of $\mathbf{C}_{P,mn}$ is presented in Section. IX-A, and the matrix forms of $\mathbf{C}_{O,mn1}$ and $\mathbf{C}_{O,mn2}$ are presented in Section. IX-B.
M Rigid Transformation Step For clarity, we retain the terms in (7) that are related with $d\mathbf{R}$ and $d\mathbf{t}$,

$$Q(d\mathbf{R}, d\mathbf{t}) = \sum_{n=1}^{N}\sum_{m=1}^{M}\big(\mathbf{C}_{P,mn} + \mathbf{C}_{O,mn1} + \mathbf{C}_{O,mn2}\big) \quad (8)$$

With the *Rodrigues* formula to represent a rotation matrix, i.e., $d\mathbf{R} = \mathbf{R}(\mathbf{x}(1:3))$ and $d\mathbf{t} = \mathbf{x}(4:6)$, we can use a six-dimensional vector $\mathbf{x}$ to represent the incremental rigid transformation matrix [48]. The *unconstrained optimization* problem is presented as the following:

$$\min_{\mathbf{x}}\underbrace{\sum_{n=1}^{N}\sum_{m=1}^{M}(\mathbf{C}_{P,mn} + \mathbf{C}_{O,mn})}_{\mathbf{C}} \quad (9)$$

where $\mathbf{C}_{O,mn} = \mathbf{C}_{O,mn1} + \mathbf{C}_{O,mn2}$ represents the part that is related with the normal vectors in the objective function. In this way we convert the constrained optimization problem of ($d\mathbf{R}, d\mathbf{t}$) into an unconstriained optimization one of $\mathbf{x}$ (note that it is different from the data point $\mathbf{x}_n$). In what follows, we present the gradients of the objective function $\mathbf{C}$.
The Gradient of the Objective Function Let $\nabla\mathbf{C}$ denotes the gradient of $\mathbf{C}$ in (9) with respect to $\mathbf{x}$, i.e. $\frac{\partial\mathbf{C}}{\partial\mathbf{x}}$. We can

now write $\nabla \mathbf{C}$ as

$$\nabla \mathbf{C} = \sum_{n=1}^{N} \sum_{m=1}^{M} \Big(\nabla \mathbf{C}_{P,mn} + \nabla \mathbf{C}_{O,mn} \Big) \tag{10}$$

where $\mathbf{C}_{P,mn} = \big[\mathbf{J}_{\mathbf{C}_{P,mn},d\theta}, \mathbf{J}_{\mathbf{C}_{P,mn},d\mathbf{t}}\big]^{\mathsf{T}}$ and $\mathbf{C}_{O,mn} = \big[\mathbf{J}_{\mathbf{C}_{O,mn},d\theta}, \mathbf{0}_{1\times 3}\big]^{\mathsf{T}}$, where $\mathbf{J}_{\mathbf{C}_{P,mn},d\boldsymbol{\theta}}$ and $\mathbf{J}_{\mathbf{C}_{P,mn},d\mathbf{t}}$ denote the Jacobian vector of $\mathbf{C}_{P,mn}$ with respect to $d\boldsymbol{\theta}$ and $d\mathbf{t}$, and $\mathbf{J}_{\mathbf{C}_{O,mn},d\boldsymbol{\theta}}$ denotes the Jacobian vector of $\mathbf{C}_{O,mn}$ with respect to $d\boldsymbol{\theta}$

$$\begin{cases} \mathbf{J}_{\mathbf{C}_{P,mn},d\boldsymbol{\theta}} = \left[\dfrac{\partial \mathbf{C}_{P,mn}}{\partial d\theta_1}, \dfrac{\partial \mathbf{C}_{P,mn}}{\partial d\theta_2}, \dfrac{\partial \mathbf{C}_{P,mn}}{\partial d\theta_3} \right] \\ \mathbf{J}_{\mathbf{C}_{P,mn},d\mathbf{t}} = \left[\dfrac{\partial \mathbf{C}_{P,mn}}{\partial dt_1}, \dfrac{\partial \mathbf{C}_{P,mn}}{\partial dt_2}, \dfrac{\partial \mathbf{C}_{P,mn}}{\partial dt_3} \right] \\ \mathbf{J}_{\mathbf{C}_{O,mn},d\boldsymbol{\theta}} = \left[\dfrac{\partial \mathbf{C}_{O,mn}}{\partial d\theta_1}, \dfrac{\partial \mathbf{C}_{O,mn}}{\partial d\theta_2}, \dfrac{\partial \mathbf{C}_{O,mn}}{\partial d\theta_3} \right] \end{cases} \tag{11}$$

We now derive the expression of $\frac{\partial \mathbf{C}_{P,mn}}{\partial d\theta_i}(i = 1,2,3)$ and $\frac{\partial \mathbf{C}_{O,mn1}}{\partial d\theta_i}(i = 1,2,3)$: $\frac{\partial \mathbf{C}_{P,mn}}{\partial d\theta_i} = \text{trace}\Big(\big(\frac{\partial \mathbf{C}_{P,mn}}{\partial d\mathbf{R}}\big)^{\mathsf{T}} \frac{\partial d\mathbf{R}}{\partial d\theta_i} \Big)$, $\frac{\partial \mathbf{C}_{O,mn1}}{\partial d\theta_i} = \text{trace}\Big(\big(\frac{\partial \mathbf{C}_{O,mn1}}{\partial d\mathbf{R}}\big)^{\mathsf{T}} \frac{\partial d\mathbf{R}}{\partial d\theta_i} \Big)$ where $\frac{\partial \mathbf{C}_{P,mn}}{\partial d\mathbf{R}} \in \mathbb{R}^{3\times 3}$ and $\frac{\partial \mathbf{C}_{O,mn1}}{\partial d\mathbf{R}} \in \mathbb{R}^{3\times 3}$ are given in the Jacobian style, trace() is the operation to compute the trace of a matrix. The readers are noted that the detailed expressions of $\frac{\partial d\mathbf{R}}{\partial d\theta_i}(i = 1,2,3)$ are presented in our prior work [56]. On the other hand, with the chain rule of matrix derivative, $\frac{\partial \mathbf{C}_{P,mn}}{\partial dt_i} = \text{trace}\Big(\big(\frac{\partial \mathbf{C}_{P,mn}}{\partial d\mathbf{t}}\big)^{\mathsf{T}} \frac{\partial d\mathbf{t}}{\partial dt_i} \Big)$. The expressions of $\frac{\partial \mathbf{C}_{P,mn}}{\partial d\mathbf{R}}$, $\frac{\partial \mathbf{C}_{P,mn}}{\partial d\mathbf{t}}$, $\frac{\partial \mathbf{C}_{O,mn1}}{\partial \partial d\mathbf{R}}$ and $\frac{\partial \mathbf{C}_{O,mn2}}{\partial \partial d\theta_j}$ are presented in Section. IX-C.

With the gradients $\nabla \mathbf{C}$ in (10) computed, the optimization problem with respect to $\mathbf{x}$ in (9) can be readily solved with a certain optimizer. Then $d\mathbf{R}$ and $d\mathbf{t}$ can be easily recovered from $\mathbf{x}$. The updated rigid transformation $\mathbf{R}^q, \mathbf{t}^q$ are computed as follows, $\mathbf{R}^q = d\mathbf{R}\mathbf{R}^{q-1}$, and $\mathbf{t}^q = d\mathbf{R}\mathbf{t}^{q-1} + d\mathbf{t}$.

M Covariance Step By solving $\frac{\partial Q}{\partial \boldsymbol{\Sigma}} = \mathbf{0}$ in (7), we can update the covariance matrix $\boldsymbol{\Sigma}^q$ as $\frac{\sum_{n=1}^{N}\sum_{m=1}^{M} p^q_{mn} \mathbf{z}^q_{mn} (\mathbf{z}^q_{mn})^{\mathsf{T}}}{N^q_{\mathbf{P}}}$, where $N^q_{\mathbf{P}} = \sum_{n=1}^{N}\sum_{m=1}^{M} p^q_{mn}$ and $\mathbf{z}^q_{mn} = \mathbf{R}^q \mathbf{y}_m + \mathbf{t}^q - \mathbf{x}_n$. The compact matrix form of $\boldsymbol{\Sigma}^q$ is presented as follows, $\Big(\mathbf{X}\text{diag}(\mathbf{P}^{\mathsf{T}}\mathbf{e})\mathbf{X}^{\mathsf{T}} - \mathbf{X}\mathbf{P}^{\mathsf{T}}\mathbf{e}(\mathbf{t}^q)^{\mathsf{T}} - \mathbf{t}^q\mathbf{e}^{\mathsf{T}}\mathbf{P}\mathbf{X}^{\mathsf{T}} + \mathbf{R}^q\mathbf{Y}\mathbf{P}\mathbf{e}(\mathbf{t}^q)^{\mathsf{T}}$ $+ (\mathbf{t}^q)\mathbf{e}^{\mathsf{T}}\mathbf{P}^{\mathsf{T}}\mathbf{Y}^{\mathsf{T}}(\mathbf{R}^q)^{\mathsf{T}} - \mathbf{R}^q\mathbf{Y}\mathbf{P}\mathbf{X}^{\mathsf{T}} - \mathbf{X}\mathbf{P}^{\mathsf{T}}\mathbf{Y}^{\mathsf{T}}(\mathbf{R}^q)^{\mathsf{T}}$ $+ \mathbf{t}^q(\mathbf{t}^q)^{\mathsf{T}} N^q_{\mathbf{P}} + \mathbf{R}^q\mathbf{Y}\text{diag}(\mathbf{P}\mathbf{e})\mathbf{Y}\mathbf{P}^{\mathsf{T}}(\mathbf{R}^q)^{\mathsf{T}} \Big) / N^q_{\mathbf{P}}$.

M-κ Step The expression $Q(\kappa)$ that is related with κ in the objective function in (7) is reduced to the following,

$$Q(\kappa) = -\kappa \sum_{n=1}^{N}\sum_{m=1}^{M} p^q_{mn} (\mathbf{R}^q \widehat{\mathbf{y}}_m)^{\mathsf{T}} \widehat{\mathbf{x}}_n + N^q_p \log c(\kappa, \beta) \tag{12}$$

whose gradient vector is $\frac{\partial Q(\kappa)}{\partial \kappa} = -\sum_{n=1}^{N}\sum_{m=1}^{M} p^q_{mn} (\mathbf{R}^q \widehat{\mathbf{y}}_m)^{\mathsf{T}} \widehat{\mathbf{x}}_n + N^q_p \frac{\partial c(\kappa,\beta)}{\partial \kappa}$. To compute $\frac{\partial c(\kappa,\beta)}{\partial \kappa}$, we use the approximate version of $c(\kappa,\beta)$ as $c(\kappa,\beta) = 2\pi e^{\kappa}[\kappa^2 - 4\beta^2]^{-\frac{1}{2}}$, whose gradient is $\frac{\partial c(\kappa,\beta)}{\partial \kappa} = 1 - (\kappa^2 - 4\beta^2)^{-1}\kappa$. By solving the equation $\frac{\partial c(\kappa,\beta)}{\partial \kappa} = 0$ with the fixed-point scheme, we can get κ^q.

M-β step The expression that is related with β in the objective function in (7), $Q(\beta)$, is presented as follows, $Q(\beta) = \beta \sum_{n=1}^{N}\sum_{m=1}^{M} p^q_{mn}((\widehat{\boldsymbol{\gamma}}^{\mathsf{T}}_{2m}(\mathbf{R}^q)^{\mathsf{T}}\widehat{\mathbf{x}}_n)^2 - (\widehat{\boldsymbol{\gamma}}^{\mathsf{T}}_{1m}(\mathbf{R}^q)^{\mathsf{T}}\widehat{\mathbf{x}}_n)^2)$
$+ N_p \log c(\kappa,\beta)$ whose gradient with respect to β is as follows, $\frac{\partial Q(\beta)}{\partial \beta} = \sum_{n=1}^{N}\sum_{m=1}^{M} p_{mn} \Big((\widehat{\boldsymbol{\gamma}}^{\mathsf{T}}_{2m}(\mathbf{R}^q)^{\mathsf{T}}\widehat{\mathbf{x}}_n)^2 - (\widehat{\boldsymbol{\gamma}}^{\mathsf{T}}_{1m}(\mathbf{R}^q)^{\mathsf{T}}\widehat{\mathbf{x}}_n)^2 \Big) + N^q_p \frac{1}{c(\kappa,\beta)} \frac{\partial c(\kappa,\beta)}{\partial \beta}$, where $\frac{\partial c(\kappa,\beta)}{\partial \beta} = 4\beta(\kappa^2 - 4\beta^2)^{-1}$. Thus, we can easily get the updated β^q by solving $\frac{\partial Q(\beta)}{\partial \beta} = 0$.

The above **E-Step** and **M-Steps** will iterate until convergence or a certain number of iterations is reached.

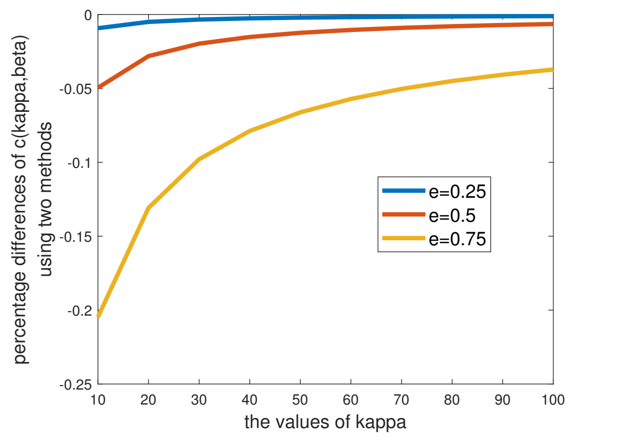

Fig. 1. The percentage differences of the normalizing constants' values computed with the two approaches. Three different cases are tested: $e = 0.25$, $e = 0.5$, $e = 0.75$.

VI. Implementation Details

The exact formular for calculating the normalizing constant $c(\kappa,\beta)$ in the Kent distribution is: $c(\kappa,\beta) = 2\pi \sum_{j=0}^{\infty} \frac{\Gamma(j+\frac{1}{2})}{\Gamma(j+1)} \beta^{2j} \left(\frac{1}{2}\kappa\right)^{-2j-\frac{1}{2}} I_{2j+\frac{1}{2}}(\kappa)$, where Γ and $I_v(\kappa)$ represent the Gamma and modified Bessel function of first kind, respectively. In real engineering implementations, we cannot sum the terms with the index from $j = 0$ to ∞. We empirically sum the terms from $j = 0$ to 99. The approximate formula of calculating $c(\kappa,\beta)$ as the following [54]: $c(\kappa,\beta) \cong 2\pi e^{\kappa}[(\kappa - 2\beta)(\kappa + 2\beta)]^{-\frac{1}{2}}$. Fig. 1 shows the percentage differences of the normalizing constants using the above two methods. As it is shown in Fig. 1, the percentage differences between the two constants will converge to zero as κ becomes larger and e becomes smaller. The eccentricity e takes values on the interval [0, 1) and controls the ellipticity parameter β as $\beta = e\frac{\kappa}{2}$. In this paper, we choose to use *the second approximated method* of computing $c(\kappa,\beta)$. We initialize the rigid transformation matrix as: $\mathbf{R}^0 = \mathbf{I}_{3\times 3}$, $\mathbf{t}^0 = \mathbf{0}_{3\times 1}$, the positional covariance matrices $\boldsymbol{\Sigma}^0$ is initialized to be large (e.g., $\boldsymbol{\Sigma}^0 = diag([100, 100, 100])$), whereas the concentration parameters κ^0 to be small (e.g. $\kappa^0 = 10$ which means large variances in normal vectors); the ellipticity parameter β^0 is initialized to be zero, which

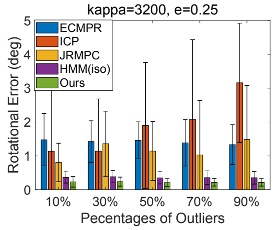

(a) Rotational error, κ=3200, e=0.25.

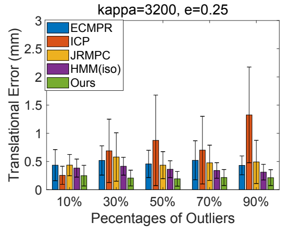

(b) Translation error, κ=3200, e=0.25.

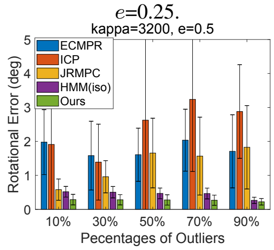

(c) Rotational error, κ=3200, e=0.5.

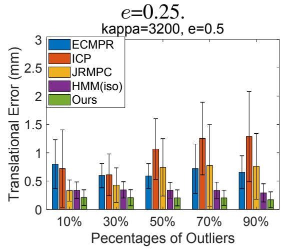

(d) Translation error, κ=3200, e=0.5.

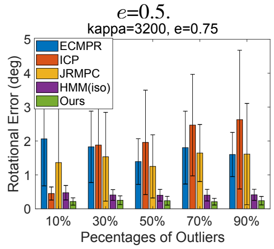

(e) Rotational error, κ=3200, e=0.75.

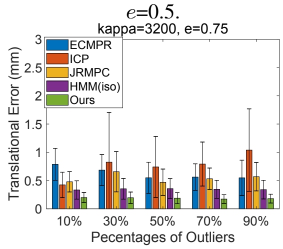

(f) Translation error, κ=3200, e=0.75.

Fig. 2. The registration error results on the femur point set, kappa =3200. The first column is the rotational error statistics while the second stores the translational error values.

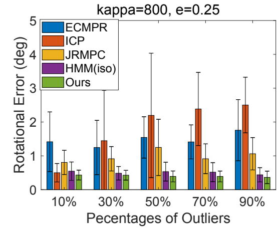

(a)Rotational error, κ=800, e=0.25.

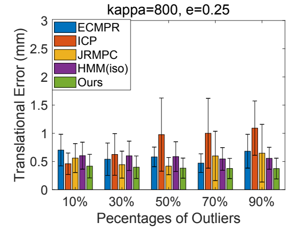

(b)Translation error, κ=800, e=0.25.

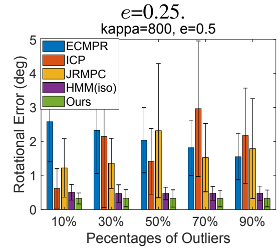

(c)Rotational error, κ=800, e=0.5.

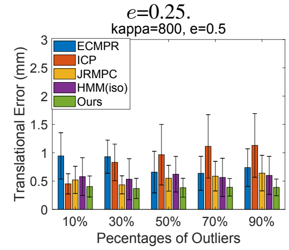

(d)Translation error, κ=800, e=0.5.

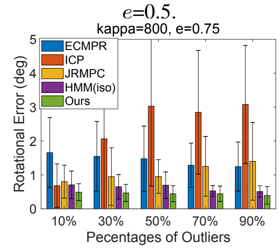

(e) Rotational error, κ=800, e=0.75.

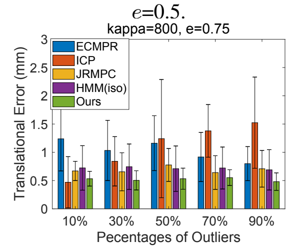

(f) Translation error, κ=800, e=0.75.

Fig. 3. The registration error results on the femur point set, kappa =800. The first column is the rotational error statistics while the second stores the translational error values.

means the orientation vectors are considered to be isotropic at the beginning of the algorithm.

VII. Experiments and Results

To verify the effectiveness, robustness and accuracy of our proposed algorithm, we validate our algorithm on two data sets: pelvis and femur data sets in the background of computer-assisted orthopedic surgery (CAOS) [46], [47]. In this scenario, the preoperative model acts as the model PS $\mathbf{D}_y$ while the intra-operative data acts as the data PS $\mathbf{D}_x$. The number of points in $\mathbf{D}_y$ is $M = 1568$ while the number of inlier points in $\mathbf{D}_x$ is $N_{\text{inliers}} = 100$. In all the experiments, between $\mathbf{D}_x$ and $\mathbf{D}_y$, the rotational degrees of $\mathbf{R}_{\text{true}}$ lie in $[10, 20]^\circ$ and the translation vectors' magnitudes lie in $[10, 20]$mm as those settings in [47]. We compare several state-of-the-art registration methods with our proposed approach: ICP [57], ECMPR [33], JRMPC [35], HMM(Isotropic) [46], [47]. The first three registration methods utilize only the positional information $\mathbf{X}$ and $\mathbf{Y}$ while HMM(Iso) and our method utilize $\mathbf{D}_x$ and $\mathbf{D}_y$. In HMM(Iso), both the positional and orientational uncertainties are isotropic.

To test and verify the registration method's robustness to noise and outliers, noise and different percentages of outliers are injected into $\mathbf{D}_x$. The anisotropic positional covariance matrix is set to be $\mathbf{\Sigma} = \text{diag}([\frac{1}{11}, \frac{1}{11}, \frac{9}{11}])$. Five different percentages of outliers are tested: 10%, 30%, 50%, 70% and 90%. More specifically, for example, in all there are $N = 100 + 100 \times 0.1 = 110$ points in $\mathbf{D}_x$ when 10% outliers are injected. In addition, we test the registration methods' under different cases of orientational error under different magnitudes and anisotropies (a) $\kappa = 800$, $e = 0.25, 0.5, 0.75$; (b) $\kappa = 3200$, $e = 0.25, 0.5, 0.75$. As indicated in [51], on one hand, $\kappa = 3200$ corresponds to 1° standard deviation while $\kappa = 800$ corresponds to 2° standard deviation. On the other hand, larger values of β (i.e., larger $e = 2\frac{\beta}{\kappa}$) indicates larger anisotropy associated with the normal vectors $\widehat{\mathbf{X}}$. For each test case with specific noise and outliers, $N_{trial} = 1000$ registration trials are tested. The rotational error in degree is computed as $\theta_{\text{err}}^{\text{deg}} = \frac{\arccos[\frac{\text{trace}(\mathbf{R}_{\text{true}}\mathbf{R}_{\text{err}}^{\mathsf{T}})-1}{2}]}{\pi} \times 180^\circ$ and the translation error in milimeter is computed as $\mathbf{t}_{\text{err}} = ||\mathbf{t}_{\text{cal}} - \mathbf{t}_{\text{true}}||$. The mean and standard deviation of both rotational and translation error values are computed and further plotted.

Fig. 2 and Fig. 3 show the rotational and translational error values when $\kappa = 3200$ and $\kappa = 800$ respectively, where the *femur* PS is used. Fig. 4 show the rotational and translational error values when $\kappa = 800$ respectively, where the *pelvis* PS is used. Two pieces of information are conveyed from the above results: our proposed algorithm (1) is able to achieve the lowest rotational and translation vector values among the

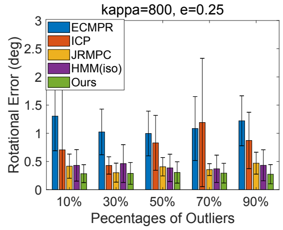

(a) Rotational error, κ=800, e=0.25.

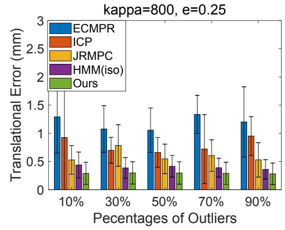

(b) Translation error, κ=800, e=0.25.

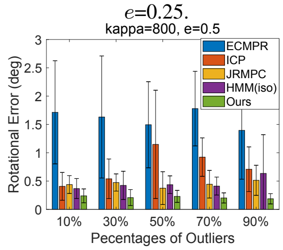

(c) Rotational error, κ=800, e=0.5.

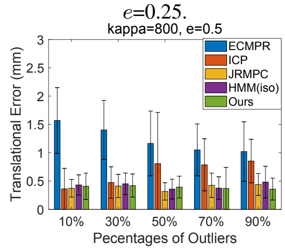

(d) Translation error, κ=800, e=0.5.

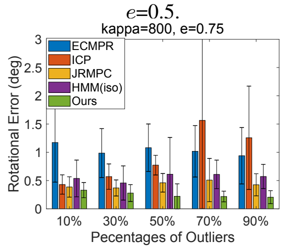

(e) Rotational error, κ=800, e=0.75.

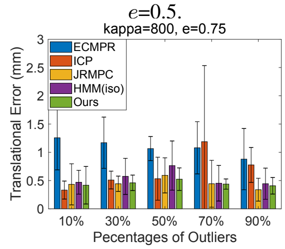

(f) Translation error, κ=800, e=0.75.

Fig. 4. The registration error results on the pelvis point set, kappa=800. The first column shows the rotational error statistics while the second shows the translational error values.

compared methods in almost all cases; (2) is very robust to noise and outliers. It should also be noted that HMM (Iso) method and our presented algorithm outperform the other three methods because that more information (i.e. the normal vectors) is utilized. Because we consider the anisotropic characteristic in both the positional and normal vectors, our proposed method owns superior performance compared to HMM(Iso). By comparing the results in Fig. 2 and those in Fig. 3, we can also conclude that both HMM(Iso) and our method achieve larger registration error values with larger error in normal vectors (i.e. smaller κ).

VIII. Conclusions

A novel, robust and accurate probabilistic rigid point set registration algorithm for computer assisted orthopaedic surgery (CAOS) is presented in this paper. The main novelty lies in considering the *anisotropy* in both the positional and orientational error. Experimental results have demonstrated the effectiveness and significantly improved performances of our approach over the state-of-the-art methods, and shows great potential clincal values.

IX. Appendix

A. The Matrix Form of $\sum_{n=1}^{N}\sum_{m=1}^{M}\mathbf{C}_{P,mn}$ in (7)

In this Appendix, we derive and present the matrix form of $\sum_{n=1}^{N}\sum_{m=1}^{M}\mathbf{C}_{P,mn}$ in (7) as $\sum_{n=1}^{N}\sum_{m=1}^{M}\mathbf{C}_{P,mn} = -\frac{1}{2}\Big(\text{trace}(\mathbf{P}^\top\mathbf{Y}^\top\mathbf{R}^\top d\mathbf{R}^\top\boldsymbol{\Sigma}^{-1}\mathbf{X}) + \text{trace}\big(\mathbf{P}\mathbf{X}^\top\boldsymbol{\Sigma}^{-1}d\mathbf{R}\mathbf{R}\mathbf{Y}\big) + \text{trace}\big(\mathbf{D}\mathbf{R}^\top d\mathbf{R}^\top\boldsymbol{\Sigma}^{-1}d\mathbf{R}\mathbf{R}\big) + N_p d\mathbf{t}^\top\boldsymbol{\Sigma}^{-1}d\mathbf{R}\mathbf{t} + \mathbf{e}^\top\mathbf{P}\mathbf{X}^\top\boldsymbol{\Sigma}^{-1}d\mathbf{t} + \mathbf{e}^\top\mathbf{P}\mathbf{X}^\top\boldsymbol{\Sigma}^{-1}d\mathbf{R}\mathbf{t} + \mathbf{e}^\top\mathbf{P}^\top\mathbf{Y}^\top\mathbf{R}^\top d\mathbf{R}\boldsymbol{\Sigma}^{-1}d\mathbf{R}\mathbf{t} + N_p\mathbf{t}^\top d\mathbf{R}^\top\boldsymbol{\Sigma}^{-1}d\mathbf{R}\mathbf{t} + \mathbf{e}^\top\mathbf{P}^\top\mathbf{Y}^\top\mathbf{R}^\top d\mathbf{R}^\top\boldsymbol{\Sigma}^{-1}d\mathbf{t} + N_p\mathbf{t}^\top d\mathbf{R}^\top\boldsymbol{\Sigma}^{-1}d\mathbf{t} + \mathbf{t}^\top d\mathbf{R}^\top\boldsymbol{\Sigma}^{-1}\mathbf{X}\mathbf{P}^\top\mathbf{e} + d\mathbf{t}^\top\boldsymbol{\Sigma}^{-1}\mathbf{X}^\top\mathbf{P}^\top\mathbf{e} + \mathbf{t}^\top d\mathbf{R}^\top d\mathbf{R}\mathbf{R}\mathbf{Y}\mathbf{P}\mathbf{e} + d\mathbf{t}^\top\boldsymbol{\Sigma}^{-1}d\mathbf{R}\mathbf{R}\mathbf{Y}\mathbf{P}\mathbf{e} + N_p d\mathbf{t}^\top\boldsymbol{\Sigma}^{-1}d\mathbf{t} + \kappa\text{trace}(\widehat{\mathbf{X}}\mathbf{P}^\top\widehat{\mathbf{Y}}^\top\mathbf{R}^\top d\mathbf{R}^\top)$, where *the readers should note that to save space* we use $\mathbf{R}$ and $\mathbf{t}$ to represent $\mathbf{R}^{q-1}$ and $\mathbf{t}^{q-1}$, $\mathbf{D}$ is defined as follows, $\mathbf{Y}\left[diag\left(\mathbf{Y}^\top\begin{bmatrix}1\\0\\0\end{bmatrix}\right), diag\left(\mathbf{Y}^\top\begin{bmatrix}0\\1\\0\end{bmatrix}\right), diag\left(\mathbf{Y}^\top\begin{bmatrix}0\\0\\1\end{bmatrix}\right)\right]\mathbf{E}$ where the matrix $\mathbf{E} = \begin{bmatrix}\mathbf{Pe},\mathbf{Pe},\mathbf{Pe}\\\mathbf{Pe},\mathbf{Pe},\mathbf{Pe}\\\mathbf{Pe},\mathbf{Pe},\mathbf{Pe}\end{bmatrix} \in \mathbb{R}^{3M\times 3}$, and $\mathbf{e}$ is the vector whose all elements are one with the appriopriate dimensions, diag is the operation that constructs a diagonal matrix from a vector.

B. The Matrix Form of $-\sum_{n=1}^{N}\sum_{m=1}^{M}\mathbf{C}_{O,mn1}$ and $-\sum_{n=1}^{N}\sum_{m=1}^{M}\mathbf{C}_{O,mn2}$ in (7)

First, let us formulate two new matrix $\mathbf{A} \in \mathbb{R}^{M\times N}$ and $\mathbf{B} \in \mathbb{R}^{M\times N}$

$$\mathbf{A} = \begin{bmatrix}(d\mathbf{R}\mathbf{R}^q\widehat{\gamma}_{11})^\top\widehat{x}_1 & \cdots & (d\mathbf{R}\mathbf{R}^q\widehat{\gamma}_{11})^\top\widehat{x}_N\\ \vdots & \ddots & \vdots\\ (d\mathbf{R}\mathbf{R}^q\widehat{\gamma}_{1M})^\top\widehat{x}_1 & \cdots & (d\mathbf{R}\mathbf{R}^q\widehat{\gamma}_{1M})^\top\widehat{x}_1\end{bmatrix} \quad (13)$$

$$\mathbf{B} = \begin{bmatrix}(d\mathbf{R}\mathbf{R}^q\widehat{\gamma}_{21})^\top\widehat{x}_1 & \cdots & (d\mathbf{R}\mathbf{R}^q\widehat{\gamma}_{21})^\top\widehat{x}_N\\ \vdots & \ddots & \vdots\\ (d\mathbf{R}\mathbf{R}^q\widehat{\gamma}_{2M})^\top\widehat{x}_1 & \cdots & (d\mathbf{R}\mathbf{R}^q\widehat{\gamma}_{2M})^\top\widehat{x}_1\end{bmatrix} \quad (14)$$

whose matrix forms are $\mathbf{A} = (d\mathbf{R}\mathbf{R}^q\widehat{\boldsymbol{\Gamma}}_1)^\top\widehat{\mathbf{X}}$ and $\mathbf{B} = (d\mathbf{R}\mathbf{R}^q\widehat{\boldsymbol{\Gamma}}_2)^\top\widehat{\mathbf{X}}$, where $\widehat{\boldsymbol{\Gamma}}_1 = [\widehat{\gamma}_{11},...,\widehat{\gamma}_{1M}] \in \mathbb{R}^{3\times M}$ and $\widehat{\boldsymbol{\Gamma}}_2 = [\widehat{\gamma}_{21},...,\widehat{\gamma}_{2M}] \in \mathbb{R}^{3\times M}$. With matrices $\mathbf{A}$ and $\mathbf{B}$, $-\sum_{n=1}^{N}\sum_{m=1}^{M}\mathbf{C}_{O,mn1}$ is given as follows, $-\sum_{n=1}^{N}\sum_{m=1}^{M}\mathbf{C}_{O,mn1} = \beta\mathbf{e}^\top\Big(-\mathbf{A}\circ\mathbf{A}\circ\mathbf{P}+\mathbf{B}\circ\mathbf{B}\circ\mathbf{P}\Big)\mathbf{e}$, where $\circ$ is the Hadamard product operation of two matrices.

On the other hand, the matrix form of $-\sum_{n=1}^{N}\sum_{m=1}^{M}\mathbf{C}_{O,mn2}$ is $-\sum_{n=1}^{N}\sum_{m=1}^{M}\mathbf{C}_{O,mn2} = -\kappa\text{trace}\Big(\widehat{\mathbf{X}}\mathbf{P}^\top\widehat{\mathbf{Y}}^\top(\mathbf{R}^q)^\top d\mathbf{R}^\top\Big)$.

C. Expressions of $\frac{\partial\mathbf{C}_{P,mn}}{\partial d\mathbf{R}}$, $\frac{\partial\mathbf{C}_{P,mn}}{\partial d\mathbf{t}}$, $\frac{\partial\mathbf{C}_{O,mn1}}{\partial\partial d\mathbf{R}}$ and $\frac{\partial\mathbf{C}_{O,mn2}}{\partial\partial d\theta_j}$

1) $\frac{\partial\mathbf{C}_{P,mn}}{\partial d\mathbf{R}} = -p_{mn}^q(\boldsymbol{\Sigma}^{q-1})^{-1}\Big(\mathbf{x}_n(\mathbf{R}^{q-1}\mathbf{y}_m+\mathbf{t}^{q-1})^\top + d\mathbf{R}(\mathbf{R}^{q-1}\mathbf{y}_m + \mathbf{t}^{q-1})(\mathbf{R}^{q-1}\mathbf{y}_m + \mathbf{t}^{q-1})^\top + d\mathbf{t}(\mathbf{R}^{q-1}\mathbf{y}_m+\mathbf{t}^{q-1})^\top\Big)$.
2) $\frac{\partial\mathbf{C}_{P,mn}}{\partial d\mathbf{t}} - p_{mn}^q(\boldsymbol{\Sigma}^{q-1})^{-1}\Big(\mathbf{x}_n + d\mathbf{t} + d\mathbf{R}(\mathbf{R}^{q-1}\mathbf{y}_m + \mathbf{t}^{q-1})\Big)$.
3) $\frac{\partial\mathbf{C}_{O,mn1}}{\partial\partial d\mathbf{R}} = 2\beta p_{mn}^q\Big(\widehat{\mathbf{x}}_n\widehat{\mathbf{x}}_n^\top d\mathbf{R}\mathbf{R}^{q-1}\widehat{\gamma}_{1m}\widehat{\gamma}_{1m}^\top(\mathbf{R}^{q-1})^\top$- $\widehat{\mathbf{x}}_n\widehat{\mathbf{x}}_n^\top d\mathbf{R}\mathbf{R}^{q-1}\widehat{\gamma}_{1m}\widehat{\gamma}_{1m}^\top(\mathbf{R}^{q-1})^\top\Big)$.
4) $\frac{\partial\mathbf{C}_{O,mn2}}{\partial d\theta_j} = p_{mn}^q\kappa^{q-1}\text{trace}\Big(\mathbf{R}^{q-1}\widehat{\mathbf{y}}_m\widehat{\mathbf{x}}_n^\top\frac{\partial d\mathbf{R}}{\partial d\theta_j}\Big)$.

REFERENCES

[1] Z. Yaniv, "Registration for orthopaedic interventions," in *Computational Radiology for Orthopaedic Interventions*. Springer, 2016, pp. 41–70.

[2] H. Ren and P. Kazanzides, "Investigation of attitude tracking using an integrated inertial and magnetic navigation system for hand-held surgical instruments," *IEEE/ASME Transactions on Mechatronics*, vol. 17, no. 2, pp. 210–217, 2012.

[3] H. Ren, C. M. Lim, J. Wang, W. Liu, S. Song, Z. Li, G. Herbert, Z. T. H. Tse, and Z. Tan, "Computer-assisted transoral surgery with flexible robotics and navigation technologies: A review of recent progress and research challenges," *Critical Reviews in Biomedical Engineering*, vol. 41, no. 4-5, 2013.

[4] J. Ma, X. Wang, Y. He, X. Mei, and J. Zhao, "Line-based stereo slam by junction matching and vanishing point alignment," *IEEE Access*, vol. 7, pp. 181 800–181 811, 2019.

[5] J. Wu, M. Liu, Z. Zhou, and R. Li, "Fast symbolic 3-d registration solution," *IEEE Transactions on Automation Science and Engineering*, 2019.

[6] D. Zhu, Z. Min, T. Zhou, T. Li, and M. Q.-H. Meng, "An autonomous eye-in-hand robotic system for elevator button operation based on deep recognition network," *IEEE Transactions on Instrumentation and Measurement*, vol. 70, pp. 1–13, 2020.

[7] D. Zhu, Y. Fang, Z. Min, D. Ho, and M. Q.-H. Meng, "Ocr-rcnn: An accurate and efficient framework for elevator button recognition," *IEEE Transactions on Industrial Electronics*, 2021.

[8] G. Balakrishnan, A. Zhao, M. R. Sabuncu, J. Guttag, and A. V. Dalca, "Voxelmorph: A learning framework for deformable medical image registration," *IEEE Transactions on Medical Imaging*, vol. 38, no. 8, pp. 1788–1800, Aug 2019.

[9] J. Ma, J. Zhao, J. Jiang, H. Zhou, and X. Guo, "Locality preserving matching," *International Journal of Computer Vision*, vol. 127, no. 5, pp. 512–531, 2019.

[10] Y. Adagolodjo, N. Golse, E. Vibert, M. De Mathelin, S. Cotin, and H. Courtecuisse, "Marker-based registration for large deformations-application to open liver surgery," in *2018 IEEE International Conference on Robotics and Automation (ICRA)*. IEEE, 2018, pp. 1–6.

[11] Z. Min, L. Liu, and M. Q.-H. Meng, "Generalized non-rigid point set registration with hybrid mixture models considering anisotropic positional uncertainties," in *Medical Image Computing and Computer Assisted Intervention – MICCAI 2019*, D. Shen, T. Liu, T. M. Peters, L. H. Staib, C. Essert, S. Zhou, P.-T. Yap, and A. Khan, Eds. Cham: Springer International Publishing, 2019, pp. 547–555.

[12] J. Ma, X. Jiang, J. Jiang, J. Zhao, and X. Guo, "Lmr: Learning a two-class classifier for mismatch removal," *IEEE Transactions on Image Processing*, vol. 28, no. 8, pp. 4045–4059, Aug 2019.

[13] J. Ma, J. Wu, J. Zhao, J. Jiang, H. Zhou, and Q. Z. Sheng, "Non-rigid point set registration with robust transformation learning under manifold regularization," *IEEE Transactions on Neural Networks and Learning Systems*, vol. 30, no. 12, pp. 3584–3597, Dec 2019.

[14] J. J. Peoples, G. Bisleri, and R. E. Ellis, "Deformable multimodal registration for navigation in beating-heart cardiac surgery," *International journal of computer assisted radiology and surgery*, vol. 14, no. 6, pp. 955–966, 2019.

[15] Z. Min and M. Q.-H. Meng, "Robust and accurate nonrigid point set registration algorithm to accommodate anisotropic positional localization error based on coherent point drift," *IEEE Transactions on Automation Science and Engineering*, 2020.

[16] Z. Min, D. Zhu, H. Ren, and M. Q.-H. Meng, "Feature-guided nonrigid 3-d point set registration framework for image-guided liver surgery: From isotropic positional noise to anisotropic positional noise," *IEEE Transactions on Automation Science and Engineering*, 2020.

[17] Y. Fu, N. M. Brown, S. U. Saeed, A. Casamitjana, R. Delaunay, Q. Yang, A. Grimwood, Z. Min, S. B. Blumberg, J. E. Iglesias *et al.*, "Deepreg: a deep learning toolkit for medical image registration," *Journal of Open Source Software*, vol. 5, no. 55, p. 2705, 2020.

[18] N. Brown, Y. Fu, S. Saeed, A. Casamitjana, Z. M. Baum, R. Delaunay, Q. Yang, A. Grimwood, Z. Min, E. Bonmati *et al.*, "Introduction to medical image registration with deepreg, between old and new," *arXiv preprint arXiv:2009.01924*, 2020.

[19] H. Ren, E. Campos-Nanez, Z. Yaniv, F. Banovac, H. Abeledo, N. Hata, and K. Cleary, "Treatment planning and image guidance for radiofrequency ablation of large tumors," *IEEE journal of biomedical and health informatics*, vol. 18, no. 3, pp. 920–928, 2013.

[20] T. Vercauteren, M. Unberath, N. Padoy, and N. Navab, "Cai4cai: The rise of contextual artificial intelligence in computer-assisted interventions," *Proceedings of the IEEE*, 2019.

[21] J. Pan, Z. Min, A. Zhang, H. Ma, and M. Q.-H. Meng, "Multi-view global 2d-3d registration based on branch and bound algorithm," in *2019 IEEE International Conference on Robotics and Biomimetics (ROBIO)*. IEEE, 2019, pp. 3082–3087.

[22] R. H. Taylor, "Computer-integrated interventional medicine: A 30 year perspective," in *Handbook of Medical Image Computing and Computer Assisted Intervention*. Elsevier, 2020, pp. 599–624.

[23] Y. Hu, V. Kasivisvanathan, L. A. M. Simmons, M. J. Clarkson, S. A. Thompson, T. T. Shah, H. U. Ahmed, S. Punwani, D. J. Hawkes, M. Emberton, C. M. Moore, and D. C. Barratt, "Development and phantom validation of a 3-d-ultrasound-guided system for targeting mri-visible lesions during transrectal prostate biopsy," *IEEE Transactions on Biomedical Engineering*, vol. 64, no. 4, pp. 946–958, April 2017.

[24] Z. Min, D. Zhu, and M. Q.-H. Meng, "Accuracy assessment of an n-ocular motion capture system for surgical tool tip tracking using pivot calibration," in *2016 IEEE International Conference on Information and Automation (ICIA)*. IEEE, 2016, pp. 1630–1634.

[25] H. Ren, E. Campos-Nanez, Z. Yaniv, F. Banovac, H. Abeledo, N. Hata, and K. Cleary, "Treatment planning and image guidance for radiofrequency ablation of large tumors," *IEEE Journal of Biomedical and Health Informatics*, vol. 18, no. 3, pp. 920–928, May 2014.

[26] Z. Min and M. Q.-H. Meng, "General first-order tre model when using a coordinate reference frame for rigid point-based registration," in *2017 IEEE 14th International Symposium on Biomedical Imaging (ISBI 2017)*. IEEE, 2017, pp. 169–173.

[27] ——, "General first-order target registration error model considering a coordinate reference frame in an image-guided surgical system," *Medical & Biological Engineering & Computing*, vol. 58, no. 12, pp. 2989–3002, 2020.

[28] Z. Min, H. Ren, and M. Q.-H. Meng, "Statistical model of total target registration error in image-guided surgery," *IEEE Transactions on Automation Science and Engineering*, vol. 17, no. 1, pp. 151–165, 2019.

[29] P. J. Besl, N. D. McKay *et al.*, "A method for registration of 3-d shapes," *IEEE Transactions on pattern analysis and machine intelligence*, vol. 14, no. 2, pp. 239–256, 1992.

[30] J. Yang, H. Li, and Y. Jia, "Go-icp: Solving 3d registration efficiently and globally optimally," in *Proceedings of the IEEE International Conference on Computer Vision*, 2013, pp. 1457–1464.

[31] F. Pomerleau, F. Colas, R. Siegwart, and S. Magnenat, "Comparing icp variants on real-world data sets," *Autonomous Robots*, vol. 34, no. 3, pp. 133–148, 2013.

[32] A. Myronenko and X. Song, "Point set registration: Coherent point drift," *IEEE transactions on pattern analysis and machine intelligence*, vol. 32, no. 12, pp. 2262–2275, 2010.

[33] R. Horaud, F. Forbes, M. Yguel, G. Dewaele, and J. Zhang, "Rigid and articulated point registration with expectation conditional maximization," *IEEE Transactions on Pattern Analysis and Machine Intelligence*, vol. 33, no. 3, pp. 587–602, 2011.

[34] W. Tabib, C. OMeadhra, and N. Michael, "On-manifold gmm registration," *IEEE Robotics and Automation Letters*, vol. 3, no. 4, pp. 3805–3812, Oct 2018.

[35] G. D. Evangelidis and R. Horaud, "Joint alignment of multiple point sets with batch and incremental expectation-maximization," *IEEE Transactions on Pattern Analysis and Machine Intelligence*, 2017.

[36] H. Yang and L. Carlone, "A polynomial-time solution for robust registration with extreme outlier rates," *Robotics: Science and Systems (RSS)*, 2019.

[37] J. Luo, S. Frisken, I. Machado, M. Zhang, S. Pieper, P. Golland, M. Toews, P. Unadkat, A. Sedghi, H. Zhou *et al.*, "Using the variogram for vector outlier screening: application to feature-based image registration," *International journal of computer assisted radiology and surgery*, vol. 13, no. 12, pp. 1871–1880, 2018.

[38] P. Babin, P. Giguere, and F. Pomerleau, "Analysis of robust functions for registration algorithms," in *2019 International Conference on Robotics and Automation (ICRA)*. IEEE, 2019, pp. 1451–1457.

[39] Y. Wang and J. M. Solomon, "Deep closest point: Learning representations for point cloud registration," in *Proceedings of the IEEE International Conference on Computer Vision*, 2019, pp. 3523–3532.

[40] ——, "Prnet: Self-supervised learning for partial-to-partial registra-

tion," in *Advances in Neural Information Processing Systems*, 2019, pp. 8814–8826.
[41] G. D. Pais, S. Ramalingam, V. M. Govindu, J. C. Nascimento, R. Chellappa, and P. Miraldo, "3dregnet: A deep neural network for 3d point registration," in *Proceedings of the IEEE/CVF Conference on Computer Vision and Pattern Recognition*, 2020, pp. 7193–7203.
[42] C. Choy, W. Dong, and V. Koltun, "Deep global registration," in *Proceedings of the IEEE/CVF Conference on Computer Vision and Pattern Recognition*, 2020, pp. 2514–2523.
[43] W. Yuan, B. Eckart, K. Kim, V. Jampani, D. Fox, and J. Kautz, "Deepgmr: Learning latent gaussian mixture models for registration," *arXiv preprint arXiv:2008.09088*, 2020.
[44] Y. Aoki, H. Goforth, R. A. Srivatsan, and S. Lucey, "Pointnetlk: Robust & efficient point cloud registration using pointnet," in *Proceedings of the IEEE Conference on Computer Vision and Pattern Recognition*, 2019, pp. 7163–7172.
[45] H. Yang, J. Shi, and L. Carlone, "Teaser: Fast and certifiable point cloud registration," *IEEE Transactions on Robotics (TRO)*, 2020.
[46] Z. Min, J. Wang, and M. Q.-H. Meng, "Robust generalized point cloud registration using hybrid mixture model," in *2018 IEEE International Conference on Robotics and Automation (ICRA)*. IEEE, 2018, pp. 4812–4818.
[47] ——, "Robust generalized point cloud registration with orientational data based on expectation maximization," *IEEE Transactions on Automation Science and Engineering*, 2019.
[48] Z. Min, J. Wang, J. Pan, and M. Q.-H. Meng, "Generalized 3-d point set registration with hybrid mixture models for computer-assisted orthopedic surgery: From isotropic to anisotropic positional error," *IEEE Transactions on Automation Science and Engineering*, 2020.
[49] J. J. Peoples and R. E. Ellis, "Composition of transformations in the registration of sets of points or oriented points," in *International Workshop on Shape in Medical Imaging*. Springer, 2020, pp. 3–17.
[50] Z. Min and M. Q.-H. Meng, "Robust generalized point set registration using inhomogeneous hybrid mixture models via expectation maximization," in *2019 International Conference on Robotics and Automation (ICRA)*. IEEE, 2019, pp. 8733–8739.
[51] S. Billings and R. Taylor, "Generalized iterative most likely oriented-point (g-imlop) registration," *International journal of computer assisted radiology and surgery*, vol. 10, no. 8, pp. 1213–1226, 2015.
[52] A. Sinha, S. D. Billings, A. Reiter, X. Liu, M. Ishii, G. D. Hager, and R. H. Taylor, "The deformable most-likely-point paradigm." *Medical image analysis*, vol. 55, pp. 148–164, 2019.
[53] S. Billings and R. Taylor, "Iterative most likely oriented point registration," in *International Conference on Medical Image Computing and Computer-Assisted Intervention*. Springer, 2014, pp. 178–185.
[54] J. T. Kent, "The fisher-bingham distribution on the sphere," *Journal of the Royal Statistical Society: Series B (Methodological)*, vol. 44, no. 1, pp. 71–80, 1982.
[55] C. M. Bishop, *Pattern recognition and machine learning*. springer, 2006.
[56] Z. Min, J. Wang, S. Song, and M. Q. . Meng, "Robust generalized point cloud registration with expectation maximization considering anisotropic positional uncertainties," in *2018 IEEE/RSJ International Conference on Intelligent Robots and Systems (IROS)*, Oct 2018, pp. 1290–1297.
[57] Z. Zhang, "Iterative point matching for registration of free-form curves and surfaces," *International journal of computer vision*, vol. 13, no. 2, pp. 119–152, 1994.